J. Bangladesh Acad. Sci. 45(1); 13-26: June 2021 DOI: 10.3329/jbas.v45i1.54256

Journal of Bangladesh Academy of Sciences

Journal homepage: http://www.bas.org.bd/publications/jbas.html

Research Article

Synthesis and characterization of a solid solution series of the type $Bi_2M_xMn_{4-x}O_{10}$ (M = Cr^{3+}, Co^{3+} and $0.0 \leq x \leq 2.0$.)

Aparna Sarker, A. K. M. Lutfor Rahman*, Tapas Debnath[1] and Altaf Hussain[2]

Department of Chemistry, Jagannath University, Dhaka, Bangladesh

ARTICLE INFO

Article History
Received: 28 January 2021
Revised: 22 May 2021
Accepted: 22 May 2021

Keywords: Solid solution, Orthorhombic phase, Glycerin nitrate method.

ABSTRACT

$Bi_2Mn_4O_{10}$ was synthesized from corresponding metal salts in glycerin by using an organic precursor-based glycerin nitrate method. The precursor was heated at various temperatures (300 – 800 °C) for about 18 hours to determine the lowest synthesis temperature for the formation of $Bi_2Mn_4O_{10}$. The XRD patterns of the calcined samples revealed that the desired mullite type phase started to form at 600 °C, which became more crystalline with further increase of calcination temperature. Attempts were also taken to prepare chromium and cobalt incorporated solid solution series with nominal composition $Bi_2M_xMn_{4-x}O_{10}$ (M = Cr^{3+} and Co^{3+}) by the same procedure. The XRD data of these series exhibited mullite type single phase up to x = 0.7 and 0.1 compositions for chromium and cobalt, respectively. For further insertion of M, an extra phase appeared along with the mullite type phase.

Introduction

Multifunctional systems are important in material research due to fundamental and technological opportunities that arise from the coupling of distinct order parameters. $Bi_2Mn_4O_{10}$ is such a type of material with multiferroic properties. $Bi_2Mn_4O_{10}$ belongs to the mullite type family (Abrahams et al., 1999; Schneider et al., 2008). It possesses the orthorhombic crystal structure with the P b a m space group (Niizeki and Wachi, 1968; Burianek et al., 2012). It resembles the crystal structure of the bismuth based mullite type $Bi_2M_4O_9$ compounds with M = Al, Fe, Ga, well explained by Debnath et al. (2010). In the structure of $Bi_2Mn_4O_{10}$, each Bi atom is surrounded by eight oxygen atoms forming BiO_8 unit as "bicapped trigonal prisms" (Munõz et al., 2002). Mn atoms are arranged in two co-ordination polyhedra: octahedral and tetragonal pyramids. The MnO_6 octahedra share their edges and form a column along the c axis. The tetragonal pyramidal MnO_5 are linked with each other by sharing their edges and form Mn_2O_8. The columns of edge-shared MnO_6 octahedra are linked by dimmers of MnO_5 tetragonal-pyramidal polyhedra through oxygen atoms. Bismuth atoms are located between the columns of the three-dimensional framework (Niizeki and Wachi, 1968; Munõz et al., 2002). In the crystal structure of $Bi_2Mn_4O_{10}$, manganese occurs in both the oxidation states: trivalent and tetravalent (Mn^{3+} and Mn^{4+}) (Nguyen et al., 1999). According to Niizeki and Wachi (1968), the correct formula of this system is to be expressed as "$Bi_2Mn_2^{3+}Mn_2^{4+}O_{10}$". Bismuth atom of $Bi_2Mn_4O_{10}$ seems not to contain stereo-chemically active lone pair electron since Bi^{3+} can easily be replaced by rare

*Corresponding author:<lrahman1973@gmail.com>

[1]Department of Theoretical and Computational Chemistry, University of Dhaka, Dhaka-1000, Bangladesh

[2]Bangabandhu Sheikh Mujibur Rahman Maritime University, Dhaka-1216, Bangladesh

earth element R^{3+} and Y^{3+}, having no lone pair electron (Kann et al., 2012). Bismuth manganate possesses commensurate magnetic property. In the crystal structure, the Mn^{3+} planes intercalate the Mn^{4+} ions are distributed along the c axis and result in alternative coupling of Mn^{4+} magnetic moments ferromagnetically and antiferroma-gnetically (Munõz et al., 2002).

Metal oxide composites, as well as pure oxides of mixed valency cations, show higher catalytic activity than simple monovalent metal oxides (Goldstein and Tseung, 1974; Fahim et al., 1981; Zaki et al., 1986). $Bi_2Mn_4O_{10}$ contains Mn atoms of different oxidation states residing in different coordination polyhedra of the same lattice. Such types of mixed oxidation states in the structure facilitate the d-d electron exchange interactions and thus provide the necessary electron-mobile environment for the surface redox activity (Hasan et al., 1999). $Bi_2Mn_4O_{10}$ was used as a catalyst in the oxidative dehydrodimerization of methane (Mamedov et al., 1994). The conductivity of $Bi_2Mn_4O_{10}$ arises due to the movement of polarons (Silva Júnior, 2010). In $Bi_2Mn_4O_{10}$, the structural voids (oxygen vacancies) are occupied by additional oxygen atoms required for charge compensation reducing the stereochemical activity of the lone electron pairs. Therefore, the doping of suitable elements in $Bi_2Mn_4O_{10}$ may improve the conductivity. The incorporation of an additional oxygen atom in the crystal structure of $Bi_2Mn_4O_{10}$ makes the structure stiffer (López-de-la-Torre et al., 2009). Hence, as a mullite type compound, $Bi_2Mn_4O_{10}$ exhibits high stability and less compressibility even at high pressure (Schneider et al., 2008). Therefore, materials having such properties have the potential to endure strong mechanical loads. The $Bi_2Mn_4O_{10}$ possesses a 223 mAh/g discharge rating capacity at 2 C current density for lithium-ion batteries (LIB) and can be a potent anode material for next-generation energy storage electrodes (Zhan and Long, 2018). It was reported that $Bi_2Mn_4O_{10}$/C composites provide high reversible specific capacity and the excellent cycling stability of LIB (Song, et al., 2018). $Bi_2Mn_4O_{10}$ is also used as promising commercial black pigments, suspended particle devices, and light valves (Saxe, 2003; Sakosae et al., 2000). Several attempts of doping in $Bi_2Mn_4O_{10}$ have already been made. $Bi_2Mn_4O_{10}$ has been synthesized using various methods viz. conventional solid-state method (Sun et al., 2006), single crystal growth (Niizeki and Wachi, 1968), co-precipitation method (Mamedov et al., 1994), urea combustion method (Ferreira et al., 2014), citric acid technique (Munõz et al., 2002), etc. But no attempts of synthesis of $Bi_2Mn_4O_{10}$ have yet been made in the "organic precursor based glycerin-nitrate method". The magnetic properties can be enhanced by doping suitable elements in $Bi_2Mn_4O_{10}$. Shukla et al. (2008) synthesized $BiMn_{2-x}Ti_xO_5$. They observed a single phase up to x = 0.5 Ti substitution at the Mn^{4+} site and the increase of net magnetic moment on this substitution. Ghosh et al. (2019) reported Nd, Sm, and Eu (denoted by R) doped $(Bi_{1-x}R_x)_2Mn_4O_{10}$ solid solution series and studied the thermal stability. They reported that the $Bi_2Mn_4O_{10}$ completely decomposed into Bi_2O_3 and Mn_3O_4 while the other $R_2Mn_4O_{10}$ form $RMnO_3$ solid solution and Mn_3O_4 on decomposition. Wu et al. (2010) prepared $Bi_{2-x}Ba_xMn_4O_{10}$ by doping Ba in the parent $Bi_2Mn_4O_{10}$ compound. Kann et al. (2012) synthesized mixed crystal $Bi_2Fe_4O_9$ -

$Bi_2Mn_4O_{10}$ through solid-state reaction method and investigated the limitation of metal cation substitution with their distribution in the crystal lattice. Mataev et al. (2013) prepared $Bi_2MeMn_4O_{10}$ (Me = Ca, Ba, Sr) at high temperature solid-state reaction. Sun et al. (2006) reported improving ferromagnetic and dielectric properties of bismuth manganate on the substitution of Bi^{3+} with Ce^{4+}. But there are no reports on Cr^{3+} and Co^{3+} incorporated $Bi_2Mn_4O_{10}$ solid solution series using organic precursor based glycerin-nitrate method. It has been reported that 13 wt% of chromium could be doped in mullite type $Bi_2Al_4O_9$ compound by the glycerin-nitrate method (Debnath et al., 2014). Therefore, in this research work an attempt was made to synthesize a new solid solution series, $Bi_2M_xMn_{4-x}O_{10}$ (M = $Cr^{3+}$and Co^{3+}) with $0.0 \leq x \leq 2.0$.

Materials and Methods

Materials

$Bi(NO_3)_3.5H_2O$ (Merck), $Mn(CH_3COO)_2.4H_2O$ (Merck), $Cr(NO_3)_3.9H_2O$ (Merck), $Co(NO_3)_2.6H_2O$ (Merck), Glycerol (Anala R), and Nitric acid (Merck) were used in this research work. All the chemicals were analytical grade and used without further purification.

Sample Preparation

All the samples were prepared by an organic precursor based glycerin nitrate method (Debnath et al., 2014; Debnath et al., 2010). $Bi(NO_3)_3.5H_2O$, $Mn(CH_3COO)_2.4H_2O$ and Glycerol were used as starting materials to prepare $Bi_2Mn_4O_{10}$. $Cr(NO_3)_3.9H_2O$ and $Co(NO_3)_2.6H_2O$ were also used to synthesize $Bi_2Cr_xMn_{4-x}O_{10}$ and $Bi_2Co_xMn_{4-x}O_{10}$ solid solution series, respectively. Appropriate molar proportions of manganese (II) acetate and nitrate salts of Bismuth, Chromium, and Cobalt were mixed in glycerin to form the gel. The resulting gel was heated at 140 °C to form a crispy precursor. The precursor was then calcined at various temperatures (300 °C to 800 °C with 100 °C intervals) for about 18 hours to determine the optimized temperature for the synthesis of the orthorhombic phase $Bi_2Mn_4O_{10}$. $Bi_2Cr_xMn_{4-x}O_{10}$ and $Bi_2Co_xMn_{4-x}O_{10}$ solid solution series were prepared using a similar procedure, and the products were washed with 0.1M HNO_3 acid after calcination.

Characterization techniques

The calcined samples were characterized using XRD, FT-IR, SEM, and EDX spectroscopic techniques. Powder X-ray diffraction patterns of the prepared samples were recorded with a Philips PW- 1380 X-ray generator operating at 40 kV-30 mA and an XDC-700 Guinier Hägg focusing camera using CuKα1 radiation. X-ray was exposed for 15 minutes on an image plate. The image plate was scanned using HD-CR 35 NDT/ CR 35 NDT scanner to get an intensity vs. line position in mm. Intensity vs. 2 theta diffraction patterns was found from the geometry of the camera. The XRD patterns are shifted vertically and shown only up to $2\theta = 10 – 70°$. FT-IR spectra were recorded using an 8400S Shimadzu spectrophotometer at 450 to 4000 cm^{-1} region. KBr was used as a reference, and 40 scanning times were done with a resolution of 1 cm^{-1}. For the sake of clarity, the FT-IR spectra are shifted vertically and presented only in the range 450 – 1000 cm^{-1}. EDX spectra were obtained with a JEOL JSM 6490 LA scanning electron microscope equipped with an EDX detector. We used the acceleration voltage of the electron gun of 20 keV, a working distance of 11 mm, and EDX and SEM collection time of 60 s and 35 s, respectively.

Results and Discussion

Optimization of temperature for the synthesis of Mullite type $Bi_2Mn_4O_{10}$ phase

The XRD patterns of the precursor of $Bi_2Mn_4O_{10}$ heating at different temperatures are shown in Fig. 1. The crystal structure of $Bi_2Mn_4O_{10}$ is orthorhombic (Niizeki and Wachi, 1968). The X-ray diffraction patterns show that the precursor possesses some tetragonal phase of Bi_2O_3 at the lower temperature (300 – 400 °C) (Perez-Mezcua et al., 2016). With the increase of temperature, this phase disappears, and the orthorhombic phase of the $Bi_2Mn_4O_{10}$ system starts to form at 600°C. At higher temperatures, the crystallinity of $Bi_2Mn_4O_{10}$ increases. The precursor gel forms a well crystalline orthorhombic phase of $Bi_2Mn_4O_{10}$ at 800 °C. The observed 2θ values of the acid-washed calcined sample at 800°C is well-matched to the reported d-values of the orthorhombic phase of $Bi_2Mn_4O_{10}$ (Niizeki and Wachi 1968). FT-IR absorption spectra of $Bi_2Mn_4O_{10}$ precursors after heat treatment at different temperatures are shown in Fig. 2. The FT-IR spectrum of $Bi_2Mn_4O_{10}$ could be characterized by distinct bands such as (i) stretching vibration into ab plane to $Mn^{4+}O_6$ chain in the range of 550 – 660 cm^{-1}(ii) movement of O_1 (bridging oxygen atoms in Mn_2O_8 dimmer) along c axis around 490-530 cm^{-1} (iii) bending of $Mn^{4+}O_6$ in the range 300 – 490 cm^{-1} (Silva Júnior, 2013). In the mid FT-IR region, the spectra above 1000 cm^{-1} appear featureless. Therefore, the spectra are shown only in the range of 450 cm^{-1} – 1000 cm^{-1}.

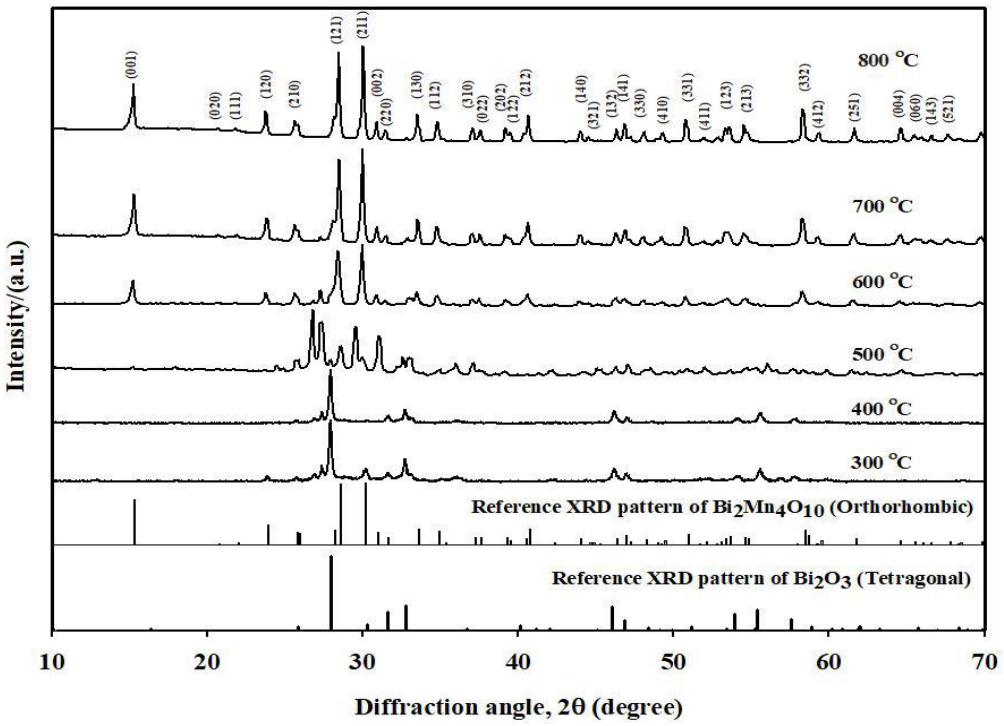

Fig. 1. XRD patterns of the precursor of $Bi_2Mn_4O_{10}$ heated at different temperatures showing a rise of orthorhombic phase at 600 °C. The reference data were collected from the literature (Niizeki and Wachi, 1968; Perez-Mezcua et al., 2016) [9008146.cif and 1545547.cif].

In our experiment, the samples do not show all the characteristic bands when calcined at temperatures below 700°C, but the characteristic bands appear at 700°C with low intensity. These bands, however, become more intense at 800°C, indicating the formation of more crystalline mullite type $Bi_2Mn_4O_{10}$ phase, which also supports the result of the XRD pattern of the sample at 800°C. Therefore, 800°C temperature has been chosen as the optimum temperature for the synthesis of all the samples ($Bi_2M_xMn_{4-x}O_{10}$) with nominal composition.

The FT-IR absorption spectra of $Bi_2Mn_4O_{10}$ calcined at 800 °C show three bands A, B, and D (Fig. 2) at 606 cm^{-1}, 578 cm^{-1}, and 462 cm^{-1}, respectively. A cluster of small band observes at 545 cm^{-1}, 528 cm^{-1}, 510 cm^{-1} and 492 cm^{-1} (denoted as C). The band A and B may be assigned as the vibration in the stretching mode of $Mn^{4+}O_6$ within the ab plane. The band C could be due to the movement of O_1 along the c axis, and band D may be due to the bending mode of vibration in $Mn^{4+}O_6$.

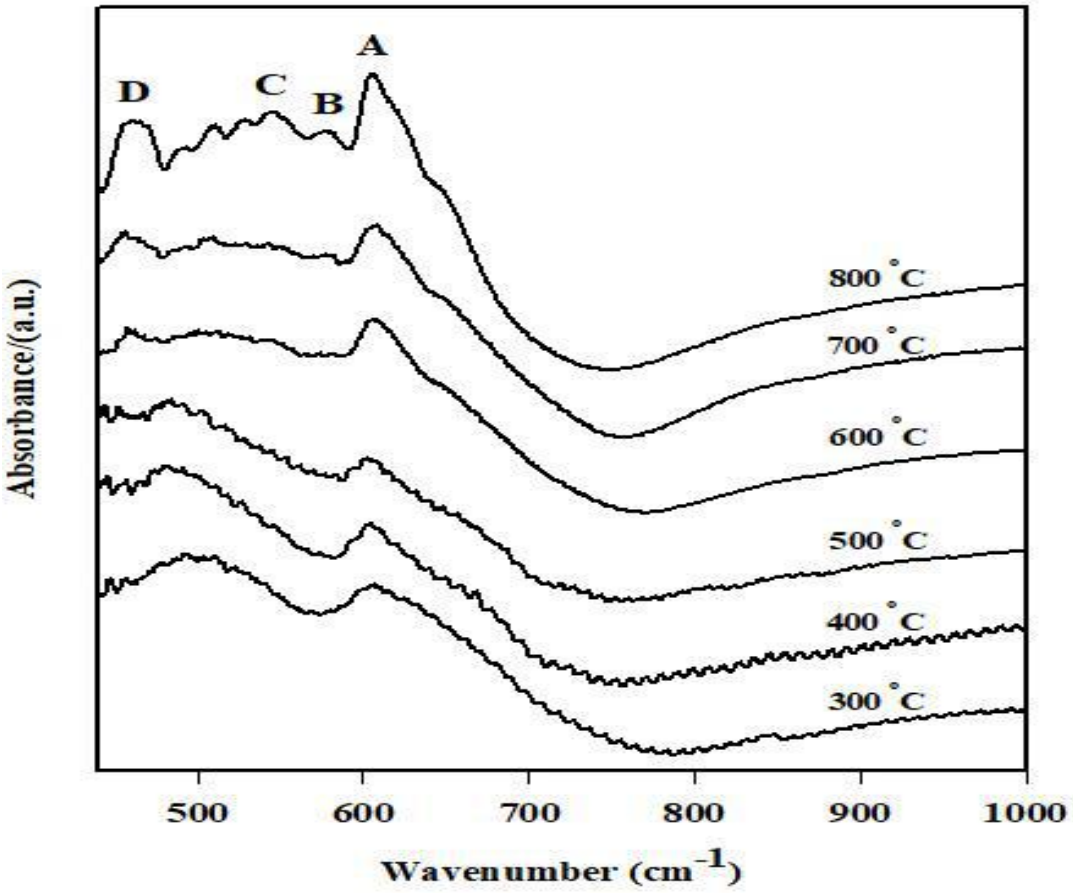

Fig. 3. Powder X-ray diffraction patterns of $Bi_2Cr_xMn_{4-x}O_{10}$ series showing single phase upto x=1.0 nominal composition. The reference data were collected from the literature (Niizeki and Wachi, 1968; Lucchesi et al., 1997) [9008146.cif and 9005291.cif].

Characterization of $Bi_2M_xMn_{4-x}O_{10}$ XRD study

The XRD patterns of the samples $Bi_2Cr_xMn_{4-x}O_{10}$ ($0.0 \leq x \leq 2.0$) and $Bi_2Co_xMn_{4-x}O_{10}$ with nominal composition ($0.0 \leq x \leq 1.0$) are shown in Fig. 3 and 4, respectively. The XRD pattern of $Bi_2Cr_xMn_{4-x}O_{10}$ shows no extra line up to x = 0.7, which indicating chromium may be inserted up to 17.5% in the orthorhombic phase of $Bi_2Mn_4O_{10}$. There are no significant changes in line positions with the increase in Cr content in the $Bi_2Cr_xMn_{4-x}O_{10}$ solid solution reveal the possibility of a very small change in cell parameters. Further increase in x, an extra phase appears along with the orthorhombic phase (*marked in Fig. 3). These additional lines are well-matched with the peaks of the reference XRD data of $Cr_{1.807}Mn_{1.193}O_4$ (Lucchesi et al., 1997). Consequently, these extra peaks in the powder XRD pattern can be indexed as a cubic phase of $Cr_{1.807}Mn_{1.193}O_4$ (Lucchesi et al., 1997). It reveals that a high amount of chromium (x>1.0) as a dopant in $Bi_2Mn_4O_{10}$ may form $Cr_{1.807}Mn_{1.193}O_4$.

However, the $Bi_2Co_xMn_{4-x}O_{10}$ samples show a single phase with up to 2.5 % (x = 0.1) insertion of Co in Fig. 4. There is also a negligible shift in lines in the XRD pattern with the increase of Co content indicating an insignificant change in cell parameters in $Bi_2Co_xMn_{4-x}O_{10}$. Some extra lines are observed even at x = 1.0 cobalt.

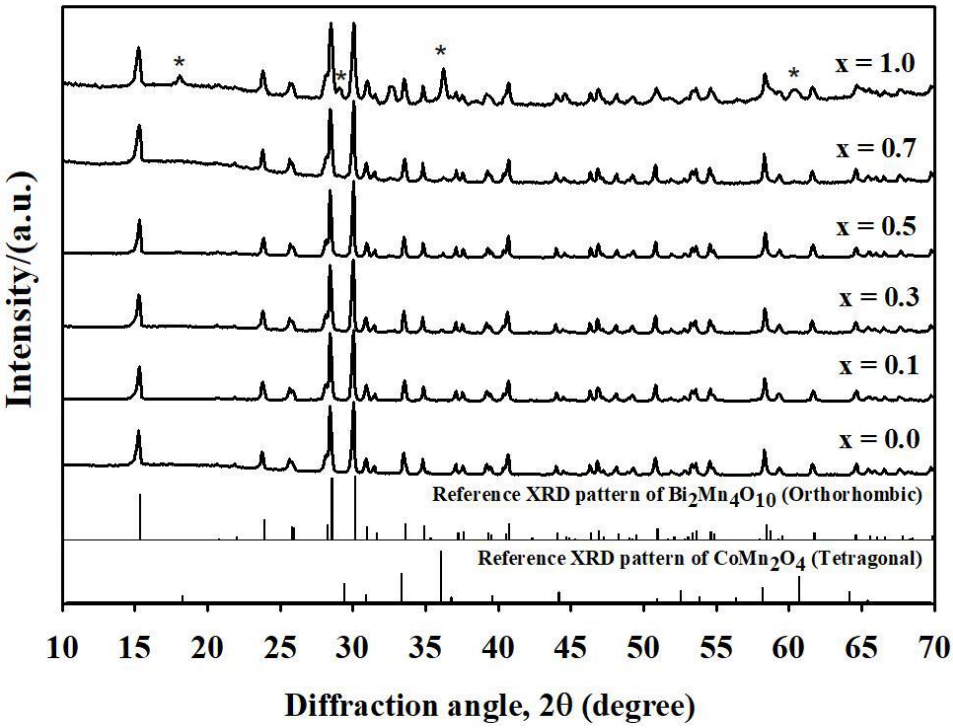

Fig. 4. Powder X-ray diffraction patterns of $Bi_2Co_xMn_{4-x}O_{10}$ series showing single phase up to x=0.1 nominal composition. The reference data were collected from the literature (Niizeki and Wachi, 1968; Yamamoto et al., 1983) [9008146.cif and 1536781.cif].

FT-IR spectroscopic study

The FT-IR spectra of $Bi_2Cr_xMn_{4-x}O_{10}$ and $Bi_2Co_xMn_{4-x}O_{10}$ are shown in Fig. 5 and 6, respectively.

All of the characteristic bands of the mullite type $Bi_2Mn_4O_{10}$ phase can be identified at the same insertion. These extra lines are almost matched with reference XRD peaks of $CoMn_2O_4$. Therefore, it can be explained that high cobalt insertion may arise tetragonal $CoMn_2O_4$ as an extra phase in this solid solution (Yamamoto et al., 1983) [1536781.cif]. band position up to x = 0.4 nominal composition of $Bi_2Cr_xMn_{4-x}O_{10}$. Further increase of Cr concentration (i.e., x> 0.4), a considerable change in the B, C, and D band groups are observed in Fig. 5. The distinct identity of B, C, and D bands start to disappear from x=1.0 chromium doping in solid solution. Samples with higher content of Cr ($x \geq 1.0$), a broadband has been identified at 487 cm^{-1} instead of separate bands C and D in $Bi_2Cr_xMn_{4-x}O_{10}$. This band becomes more intense with nominal composition x = 2.0 of $Bi_2Cr_xMn_{4-x}O_{10}$. The widening of the FT-IR band through the coalesce of characteristic band group below 550 cm^{-1} and disappearance of band at 578 cm^{-1} gradually visible with the increase of chromium. According to the literature, two absorption peaks at 516 cm^{-1} and 621 cm^{-1} are reported for Mn-O vibration frequency of the metal at tetrahedral and octahedral sites, respectively in the IR spectrum of Cr_2MnO_4 (similar to $Cr_{1.807}Mn_{1.193}O_4$) (Tong et al., 2015). The $Bi_2Mn_4O_{10}$ also contain band at 606 cm^{-1} and 510 cm^{-1} (within a cluster of small bands denoted by C).

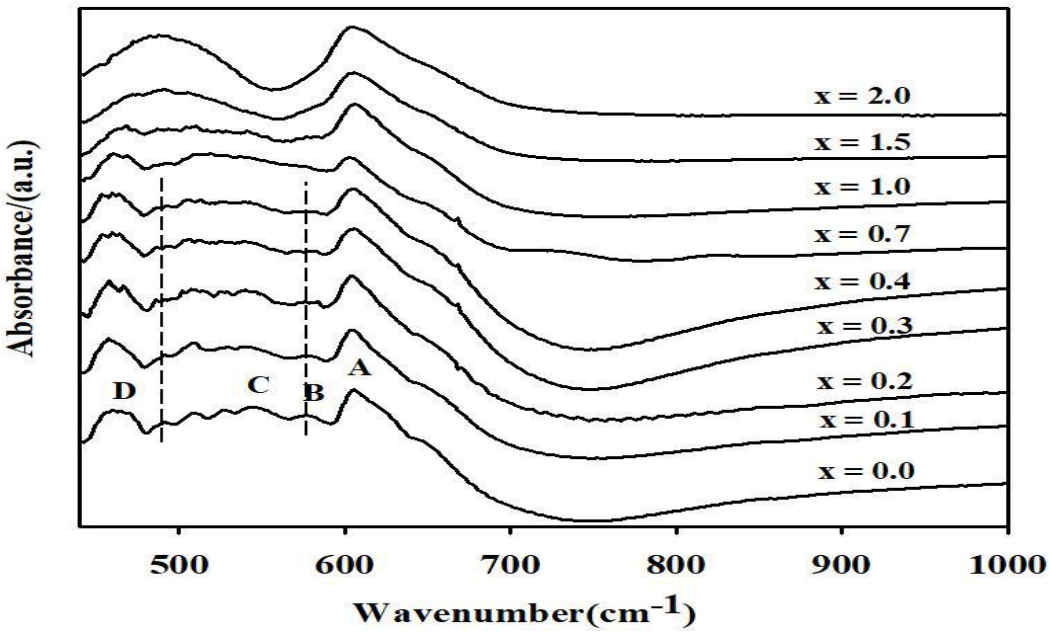

Fig. 5. FT-IR spectra of $Bi_2Cr_xMn_{4-x}O_{10}$ solid solution series illustrate recombination with broadening bands below 550 cm^{-1} and band disappearance at 580 cm^{-1}.

Therefore, after the insertion of a certain percentage of Cr, an increase of its content may cause the arise of an extra phase of $Cr_{1.807}Mn_{1.193}O_4$. It may result in a vibrational band at 516 cm^{-1} and 621 cm^{-1} those may overlap with the vibrational band for $Bi_2Cr_xMn_{4-x}O_{10}$ single phase and gets broader (Fig. 5). It reveals that the insertion of Cr may affect the movement of the bridging oxygen atom (O_1) along the c axis, which is connected to Mn^{3+} and thus enhances the octahedra's bending mode. Therefore, FT-IR data support the XRD result.

The FT-IR spectra of the $Bi_2Co_xMn_{4-x}O_{10}$ solid solution series exhibit all characteristic bands of $Bi_2Mn_4O_{10}$ below x= 0.3 shown in Fig. 6. The shifting of the band at 578 cm^{-1} is observed at $x \geq 0.3$ cobalt content and then gets disappeared at x=1.0. The broadening of the FT-IR band at 524 cm^{-1} through merging characteristic vibration bands group below 550 cm^{-1} appears at x> 0.7. Since it was reported that $CoMn_2O_4$ possess FT-IR band at 502 and 617 cm^{-1} (Hosseini et al., 2011) that have been considered as an extra phase in this study. This phenomenon of band broadening might be due to the influence of further insertion of Co in $Bi_2Mn_4O_{10}$. The peak position of band A remains the same for Cr doping compositions, while negligible shifting of this band is observed for Co doping. However, recombination and broadening of the characteristic group of FT-IR bands after a certain percentage of Cr or Co doping support the XRD results.

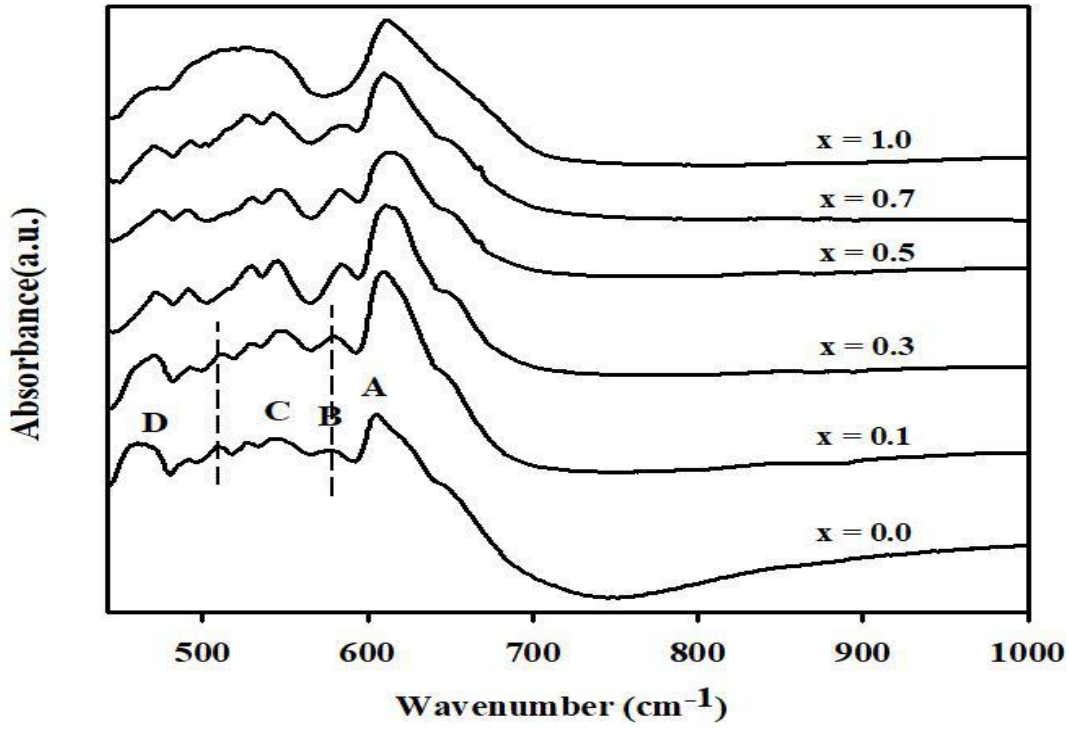

Fig. 6. FT-IR absorption spectra of $Bi_2Co_xMn_{4-x}O_{10}$ solid solution series illustrate the band's disappearance at 585 cm^{-1} and merge with broadening bands below 550 cm^{-1}.

Microscopic study

The surface morphology and microstructure of the prepared samples were characterized by scanning electron microscopy coupled with energy dispersive X-ray (SEM/EDX) spectroscopy. SEM images of some selected samples of $Bi_2Cr_xMn_{4-x}O_{10}$ and $Bi_2Co_xMn_{4-x}O_{10}$ solid solution series are shown in Fig.7 and 8, respectively.

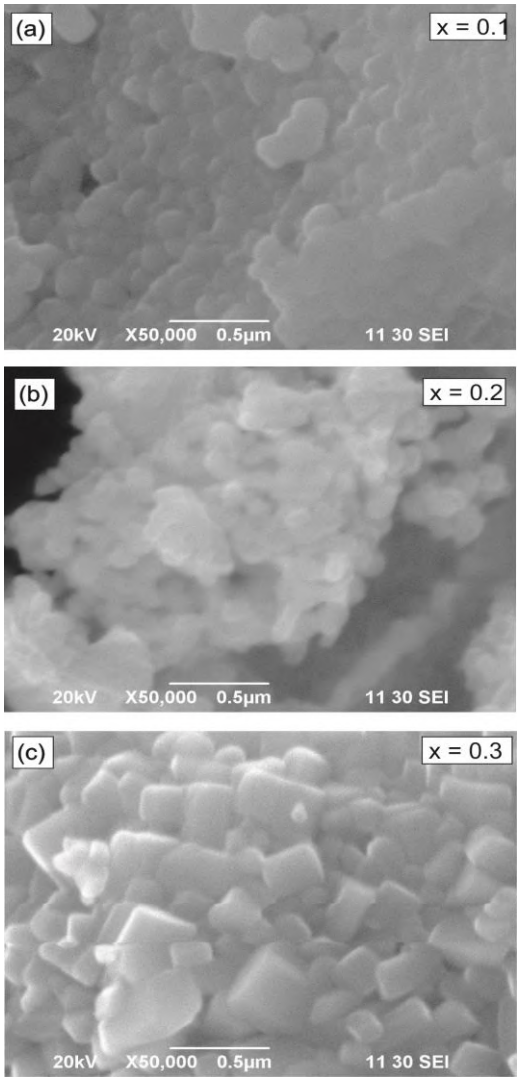

Fig. 7. SEM images of samples of $Bi_2Cr_xMn_{4-x}O_{10}$ solid solution series with doping composition (a) x = 0.1, (b) x = 0.2 and (c) x = 0.3. The samples seem polycrystalline powder.

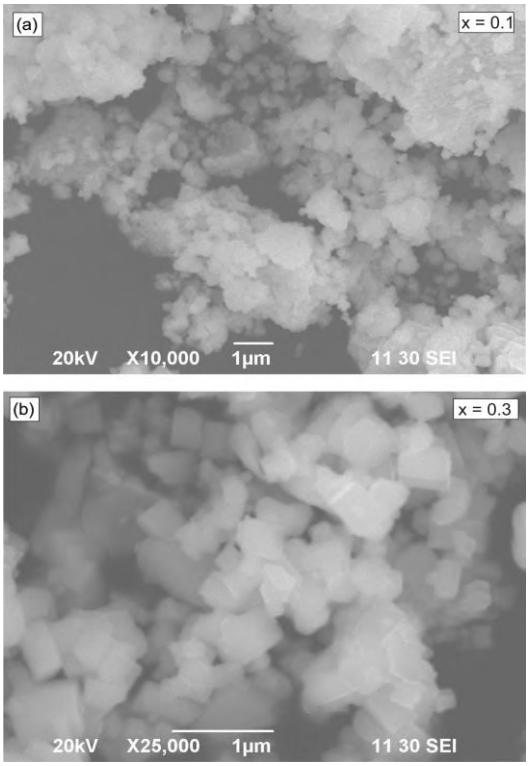

Fig. 8. SEM images of samples of $Bi_2Co_xMn_{4-x}O_{10}$ solid solution series with doping composition (a) x = 0.1 and (b) x = 0.3. The samples seem polycrystalline powder.

The micrograph of the samples of $Bi_2Cr_xMn_{4-x}O_{10}$ shows the smaller agglomerated spherical particles at x = 0.1 (Fig. 7a) doping composition. At x = 0.3 (Fig. 7c) doping composition of chromium, the particles become irregular prismatic hexagonal shape with a clear grain boundary. Similar topography is observed in the $Bi_2Co_xMn_{4-x}O_{10}$ solid solution series. At x = 0.3 (Fig. 8b) doping of cobalt, the grains seem almost cubic in shape. Both the solid solution series are polycrystalline powder, which has been observed from the SEM images.

The EDX spectra of some selected samples of $Bi_2Cr_xMn_{4-x}O_{10}$ and $Bi_2Co_xMn_{4-x}O_{10}$ are shown in Fig. 9 and 10, respectively. The spectra are shown only up to 10 keV.

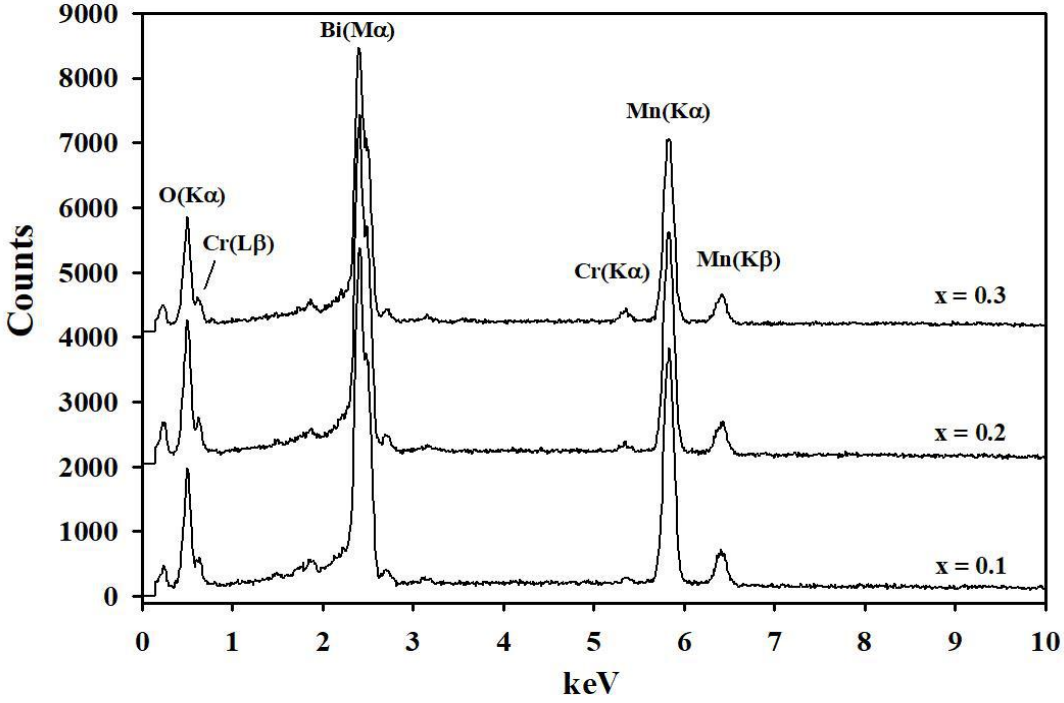

Fig. 9. EDX spectra of $Bi_2Cr_xMn_{4-x}O_{10}$ solid solution series.

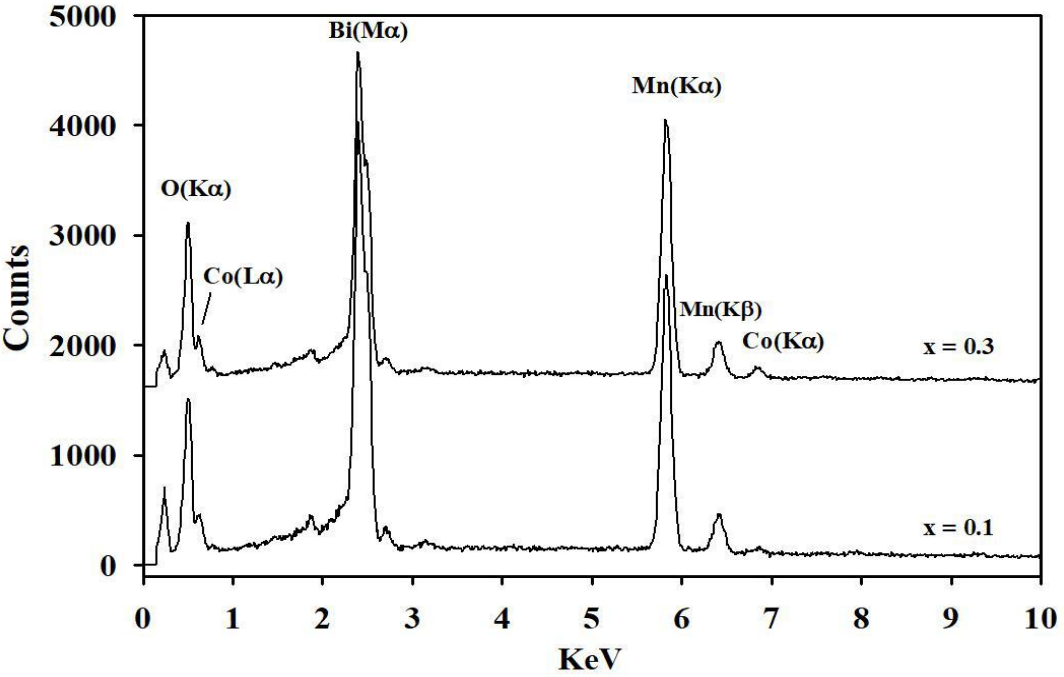

Fig. 10. EDX spectra of $Bi_2Co_xMn_{4-x}O_{10}$ solid solution series.

Seven distinct peaks in all EDX spectra at 0.525, 2.419, 5.894, and 6.414 keV are identified for O(Kα), Bi(Mα), Mn(Kα), and Mn(Kβ) lines, respectively in $Bi_2Mn_4O_{10}$ and also in doped $Bi_2Mn_4O_{10}$ samples. In addition to these peaks, samples of the $Bi_2Cr_xMn_{4-x}O_{10}$ solid solution series show peaks at 0.624 and 5.361 keV for Cr(Lβ) and Cr(Kα) lines, respectively and the peaks at 0.628 and 6.871 keV are assigned for Co(Lα) and Co(Kα), respectively for the $Bi_2Co_xMn_{4-x}O_{10}$ solid solution series. A systematic increase of intensities of Cr(Kα) and Co(Kα) peaks are observed with the nominal increase of the incorporation of Cr and Co in samples of $Bi_2M_xMn_{4-x}O_{10}$ (M = Cr and Co). The EDX study also suggests that Cr and Co may be incorporated up to a certain percentage in the orthorhombic phase of $Bi_2Mn_4O_{10}$.

The XRD and EDX data of the $Bi_2M_xMn_{4-x}O_{10}$ sample show that only a certain percentage of Chromium and Cobalt can be doped in $Bi_2Mn_4O_{10}$. Nguyen et al. (1999) reported the mixed site occupancy with a complex cation distribution for $Bi_2FeMn_3O_{10}$ presented as $Bi_2[Mn_{1.66}^{4+}Fe_{0.34}^{3+}]_{oct.}[Mn_{1.00}^{3+}Mn_{0.34}^{3+}Fe_{0.66}^{3+}]_{tet.pyd.}O_{10}$, which showed that the Fe^{3+} and Mn^{3+} preferentially occupy the tetragonal pyramidal sites and Mn^{4+} preferentially occupy the octahedral sites. Kann et al. (2012) were successful in doping Fe^{3+} partially in the $Bi_2Mn_4O_{10}$ structure due to the similarity of ionic radii of Fe^{3+} and Mn^{3+} and the tendency of small change in unit cell volume and lattice parameter for the substitution on tetragonal pyramidal sites. In the present study, a certain percentage of chromium and cobalt may be doped that involve a minimal change of cell parameter because the ionic radii of dopant i.e. Cr^{3+} and Co^{3+} are very closer to that of Mn^{3+}. Since $Bi_2Mn_4O_{10}$ tendens to retain the structural stability (López-de-la-Torre et al., 2009) further increase of chromium and cobalt content may causes the formation of an additional phase, suppose to be $Cr_{1.807}Mn_{1.193}O_4$ and $CoMn_2O_4$, respectively along with the parent solid $Bi_2Mn_4O_{10}$.

Conclusion

$Bi_2Mn_4O_{10}$ and its chromium and cobalt substituted solid solution series were synthesized using the organic precursor-based glycerin nitrate method. The investigation revealed that $Bi_2Mn_4O_{10}$ was formed with an orthorhombic phase at 600 °C. The attempt to synthesize $Bi_2M_xMn_{4-x}O_{10}$ (M = Cr and Co) using a similar method is a new approach. XRD patterns revealed that the $Bi_2Mn_4O_{10}$ type orthorhombic single phase might be prepared with up to 17.5% and 2.5% incorporation of Cr and Co, respectively. The possible partial insertion of Cr and Co in the $Bi_2Mn_4O_{10}$ orthorhombic type structure was also supported by the systematic increase of Cr(Kα) and Co(Kα) peak, in the EDX spectra of corresponding samples. FT-IR absorption spectra suggested the disorder in $Bi_2Mn_4O_{10}$ at a certain composition of the doping element ($x \geq 0.7$). SEM images of both $Bi_2Cr_xMn_{4-x}O_{10}$ and $Bi_2Co_xMn_{4-x}O_{10}$ samples were polycrystalline powder with a smaller particle size which hopefully could be used as good ceramic materials.

Conflict of Interest

The authors declared that they have no conflict of interest.

Funding Information

Partial financial support was received for this research from Jagannath University, Dhaka, Bangladesh.

Acknowledgements

We would like to thank the Centre for Advanced Research in Sciences (CARS), University of Dhaka for the instrumental support and the Department of Chemistry, University of Dhaka, Bangladesh for the logistic support in this research work.

References

Abrahams I, Bush AJ, Hawkes GE and Nunes T. Structure and oxide Ion conductivity mechanism in $Bi_2Al_4O_9$ by combined X-ray and high-resolution neutron powder diffraction and ^{27}Al solid state NMR. *J. Solid State Chem.* 1999; 147(2): 631-636.

Burianek M, Krenzel TF, Schmittner M, Schreuer J, Fischer RX, Mühlberg M, Nénert G, Schneider H and Gesing TM. Single crystal growth and characterization of mullite-type $Bi_2Mn_4O_{10}$. *Int. J. Mater. Res.* 2012; 103(4): 449-455.

Debnath T, Rüscher CH, Fielitz P, Ohmann S and Borchardt G. Series of compositions $Bi_2(M'_xM_{1-x})_4O_9$ (M, M = Al, Ga, Fe; $0 \leq x \leq 1$) with mullite-type crystal structure: Synthesis, characterization and $^{18}O/^{16}O$ exchange experiment. *J. Solid State Chem.* 2010; 183: 2582–2588.

Debnath T, Rüscher CH, Gesting TM, Fielitz P, Ohmann S and Borchardt G. Oxygen diffusion in $Bi_2M_4O_9$ (M = Al, Ga, Fe) systems and the effect of Sr doping in $Bi_{2-2x}Sr_{2x}M_4O_{9-x}$ studied by isotope exchange experiments and IR absorption. *Advances in Solid Oxide Fuel Cells VI: Ceramic Engineering and Science Proceedings.* 2010b; 31(4): 81-89.

Debnath T, Ullah A, Rüscher CH and Hussain A. Chromium substitution in mullite type bismuth aluminate: $Bi_2Cr_xAl_{4-x}O_9$ with $0 \leq x \leq 2.0$. *J. Solid State Chem.* 2014; 220: 167–171.

Fahim RB, Zaki MI and Gabr RM. Heterogeneous and/or homogeneous chromia-catalysed decomposition of hydrogen peroxide. *Surf. Technol.* 1981; 12(4): 317-326.

Ferreira RA, Elenice dosSantos M, Morilla-Santos C, Lebullenger R, Peña O and Lisboa-Filho PN. Effect of Eu substitution on the crystallographic and magnetic properties of the $BiMn_2O_5$ oxide obtained by urea combustion. *Ceram. Int.* 2014; 40(8) Part B: 13643-13648.

Ghosh K, Murshed MM and Gesing TM. Synthesis and characterization of $(Bi_{1-x}R_x)_2Mn_4O_{10}$: structural, spectroscopic and thermogravimetric analyses for R = Nd, Sm and Eu. *J. Mater. Sci.* 2019; 54(21): 13651-13659.

Goldstein J R and Tseung ACC. The kinetics of hydrogen peroxide decomposition catalyzed by cobalt-iron oxides. *J. Catal.* 1974; 32(3): 452-465.

Hasan MA, Zaki MI, Pasupulety L and Kumari K. Promotion of the hydrogen peroxide decomposition activity of manganese oxide catalysts. *Appl. Catal., A.* 1999; 181(1): 171-179.

Hosseini SA, Salari D, Niaei A, Deganello F, Pantaleo G and Hojati P. Chemical-physical properties of spinel $CoMn_2O_4$ nano-powders and catalytic activity in the 2-propanol and toluene combustion: Effect of the preparation method. *J. Environ. Sci. Health A Tox. Hazard Subst. Environ. Eng.* 2011; 46: 291–297.

Kann ZR, Auletta JT, Hearn EW, Webew SU, Becker KD, Schneider H and Lufaso MW. Mixed crystal formation and

structural studies in the mullite-type system $Bi_2Fe_4O_9$–$Bi_2Mn_4O_{10}$. *J. Solid State Chem*. 2012; 185: 62-71.

López-de-la Torre L, Friedrich A, Juarez-Arellano EA, Winkler B, Wilson DJ, Bayarjargal L, Hanfland M, Burianek M, Mühlberg M and Schneider H. High-pressure behavior of the ternary bismuth oxides $Bi_2Al_4O_9$, $Bi_2Ga_4O_9$ and $Bi_2Mn_4O_{10}$. *J. Solid State Chem.* 2009; 182(4): 767-777.

Lucchesi S, Russo U and Della GA. Crystal chemistry and cation distribution in some Mn-rich natural and synthetic spinels. *Eur. J. Mineral.* 1997; 9(1): 31-42.

Mamedov EA, Shamilov NT, Vislovskii VP, Joshi PN and Badrinarayan S. Bi_2O_3-M_2O_3 catalysts for oxidative coupling of methane: Relationship between structural features and catalytic behaviours. *Stud. Surf. Sci. Catal*. 1994; 82: 395-401.

Mataev MM, Myrzahmetova NO, Nuketaeva DZH, Zhumanova NA, Kuanysheva ZH K, Nurbekova MA and Abdraimova MR. X-ray scattering analysis of complex manganites $Bi_2MeMn_4O_{10}$ (Me- Ca, Ba, Sr). *World Appl. Sci. J.* 2013; 22 (Special Issue on Techniques and Technologies): 40-43.

Munõz A, Alonso JA, Casais MT, Martínez-Lope MJ, Martínez JL and Fernández-Díaz MT. Magnetic structure and properties of $BiMn_2O_5$ oxide: A neutron diffraction study. *Phys. Rev. B.* 2002; 65(14): 144423.

Nguyen N, Legrain M, Ducouret A and Raveau B. Distribution of Mn^{3+} and Mn^{4+} species between octahedral and square pyramidal sites in $Bi_2Mn_4O_{10}$-type structure. *J. Mater. Chem.* 1999; 9(3): 731-734.

Niizeki N and Wachi M. The crystal structures of $Bi_2Mn_4O_{10}$, $Bi_2Al_4O_9$ and $Bi_2Fe_4O_9$.*Z. Kristallogr*. 1968; 127(1-4): 173-187.

Perez-Mezcua D, Bretos I, Jimenez R, Ricote J, Jiménez-Rioboo JR, Gonçalves da Silva C, Chateigner D, Fuentes-Cobas L, Sirera R and Calzada ML. Photochemical solution processing of films of metastable phases for flexible devices: the β-Bi_2O_3 polymorph. *Sci. Rep.* 2016; 6: 39561.

Sakosae GE, Sarver JE and Novotny M. Bismuth manganese oxide pigments. European Patent. 2000; EP 1 140 704 B2.

Saxe RL. SPD films and light valves comprising liquid suspensions of heat-reflective particles of mixed metal oxides and methods of making such particles. US Patent. US 6606185 B2. 2003.

Schneider H, Schreuer J and Hildmann B. Structure and properties of mullite-A review. *J. Eur. Ceram. Soc.* 2008; 28(2): 329-344.

Shukla DK, Mollah S, Kumar R, Thakur P, Chae KH, Choi WK and Banerjee A. Effect of Ti substitution on multiferroic properties of $BiMn_2O_5$. *J. Appl. Phys.* 2008; 104(3): 033707-1-10.

Silva Júnior FM, Paschoal CWA, Almeida RM, Moreira RL, Paraguassu W, Castro Junior MC, Ayala AP, Kann ZR and Lufaso MW. Room-temperature vibrational properties of the $BiMn_2O_5$ mullite. *Vib. Spectrosc.* 2013; 66: 43-49.

Silva Júnior FM. Propriedades vibracionals e dielétricas da mulita $Bi_2Mn_4O_{10}$. Masters Thesis. Department of Physics. Federal University of Maranhão (Brazil). 2010.

Song Z, Zhang H, Feng K, Wang H, Li X and Zhang H. $Bi_2Mn_4O_{10}$: a new mullite-type anode material for lithium-ion batteries. *Dalton Trans*. 2018; 47(23): 7739-7746.

Sun ZH, Cheng BL, Dai S, Jin KJ, Zhou Y L, Lu HB, Chen ZH and Yang GZ. Effect of Ce substitution on magnetic and dielectric properties of $BiMn_2O_5$. *J. Appl. Phys. (Melville, NY, U. S.)*. 2006; 99(8): 084105.

Tong Y, Ma J, Zhao S, Huo H and Zhang H. A salt-assisted combustion method to prepare well-dispersed octahedral $MnCr_2O_4$ spinel nanocrystals, *J. Nanomater*., 2015; Article ID 214978:1-5.

Wu YJ, Wang N, Lin YQ, Liu XQ and Chen XM. Effects of Ba substitution on structure and dielectric response of $Bi_2Mn_4O_{10}$ ceramics. *Mater. Chem. Phys.* 2010; 121(1-2): 326-329.

Yamamoto N, Kawano S, Achiwa N and Higashi S. Preparation by a wet method and ionic distribution of transition metal-substituted hausmanite spinel. *J. Jpn. Soc. Powder Metall.* 1983; 30(2): 48-54.

Zaki MI, Fouad NE, Leyrer J and Knőzinger H. Physicochemical investigation of calcined chromia-coated silica and alumina catalysts: Characterization of chromium-oxygen species. *Appl. Catal.* 1986; 21(2): 359-377.

Zhan J and Long YY. Synthesis of $Bi_2Mn_4O_{10}$ nanoparticles and its anode properties for LIB. *Ceram. Int.* 2018; 44(12): 14891-14895.